Surface morphology, stress, and volume change during growth and crystallization of interface-stabilized amorphous $Fe_{100-x}Zr_x$ films

S. G. Mayr* and K. Samwer
I. Physikalisches Institut, Bunsenstrasse 9, D–37073 Göttingen, Germany
(Received 1 May 2001; revised manuscript received 14 August 2001; published 22 February 2002)

Thin $Fe_{100-x}Zr_x$ films, evaporated for $x \leqslant 7$ on top of a Zr substrate, show a glass-to-crystal transition in dependence of the film thickness. For $x > 7$ the transition does not occur, and the film grows amorphous for any film thickness. With the help of *in situ* ultrahigh-vacuum scanning-tunneling microscopy and intrinsic stress measurements during film deposition, it is possible to investigate the described phase transition quantitatively, and to estimate the volume change of the film at the critical film thickness during crystallization. This allows an interpretation of the phase transition in terms of instability criteria for the crystal-to-glass transition. Using pure Fe on Zr provides the exciting opportunity of investigating surface topographs of monoatomic amorphous thin films, commonly not accessible for experiments. Just by tuning the film composition, totally amorphous film growth can be easily compared to crystal films, keeping primarily the material system unchanged. Thus, crystal-film growth can be characterized by columnar grain growth under strong tensile stresses, and amorphous films develop accordingly mesoscopic hill-like structures.

DOI: 10.1103/PhysRevB.65.115408 PACS number(s): 68.55.−a, 61.43.Dq, 68.18.Jk

I. INTRODUCTION

For almost two decades, the growth of multilayers of metals with highly different bulk equilibrium lattice constants has attracted considerable interest, primarily triggered by the discovery of amorphous phase formation by solid state reactions.[1] The latter involves multilayered structures of two different metallic constituents, generally prepared by evaporation or sputtering, with large differences in atomic sizes, mobilities in each other and high negative heat of mixing. $Fe_{100-x}Zr_x$ has been the system of choice for numerous investigations, starting from first amorphization reactions of Clemens *et al.*,[2] primarily as—additionally besides standard characterization, e.g., by diffraction methods (e.g., Ref. 3) or resistivity measurements[4]—magnetic investigations are feasible, i.e., magnetization measurements[5–7] or conversion-electron Mössbauer spectroscopy (CEMS).[8–10] A general feature of any such system during growth is the high interface-to-volume ratio, which can have profound impacts on film structures due to the influence of surface energy and stress (both vacuum-film and film-substrate interface) and high cooling rates (see Ref. 11 for early experiments), even without solid-state amorphization taking place. Thus the formation of nonequilibrium phases, such as the amorphous phase, is possible, either due to kinetic restrictions during film deposition, or due to the fact that the interface energy is an additional contribution to the free energy, which is able to shift phases in the bulk equilibrium phase diagram. Such a high contribution to interface energy can be lattice-parameter effects present between the film and substrate. As an example, fcc Fe can be grown on fcc Cu due to comparable lattice parameters.[12] Similarly, lattice mismatchs of the crystal phases between the film and substrate can lead to a stabilization of amorphous films, as first observed for Fe/Zr by Williamson and Clemens[8] by CEMS and confirmed by magnetometric[13,5,6] or diffraction measurements[3] and reported for other multilayers of Fe with different elements, such as Ce or Gd.[14–16] With increasing film thickness, and thus decreasing contribution of the interfaces, the bulk properties—and bulk phases—dominate, and for Fe/Zr in all reported experiments, crystallization sets in above a critical threshold thickness of 1.6—2.3 nm. By choosing $Fe_{100-x}Zr_x$–alloy films, the volume driving force for crystallization can be modified[17] and it could be shown by diffraction and magnetic methods that, for $x \leqslant 7$, they grow amorphous up to a critical film thickness and crystallize polymorphously afterwards.[17,7,18] Proposing an almost constant misfit interface-energy contribution for different film compositions x, the critical film thickness t_C could be shown to obey the scaling law

$$t_C \propto \frac{1}{x_C - x}. \tag{1}$$

All of the above-mentioned investigations involve indirect surface characterization and are mostly performed *ex situ*. In the present study, the growth modes and phase transitions of these $Fe_{100-x}Zr_x$ films on Zr are investigated *in situ* using ultrahigh-vacuum (UHV) scanning-tunneling microscopy (STM) and intrinic-stress measurements (ISM), which enable first direct observations of the film growth and amorphous to crystal phase transition. Furthermore, the difference in crystal and amorphous thin film growth kinetics is studied, using $x > 7$ and high film thicknesses. In this sense, we choose the ZrFe system as a typical representative of the broad class of materials systems with amorphouslike interface structure, with thermodynamically counteracting bulk and interface effects. The paper is organized as follows: After an overview of the experimental conditions and methods, we report about direct observations of the polymorphous crystallization using STM and ISM measurements. For higher film thicknesses, and different compositions, purely crystalline or amorphous ZrFe film growth can be compared. By film deposition at different temperatures, we attribute the question, whether interdiffusion, accompanied by solid-state amorphization,

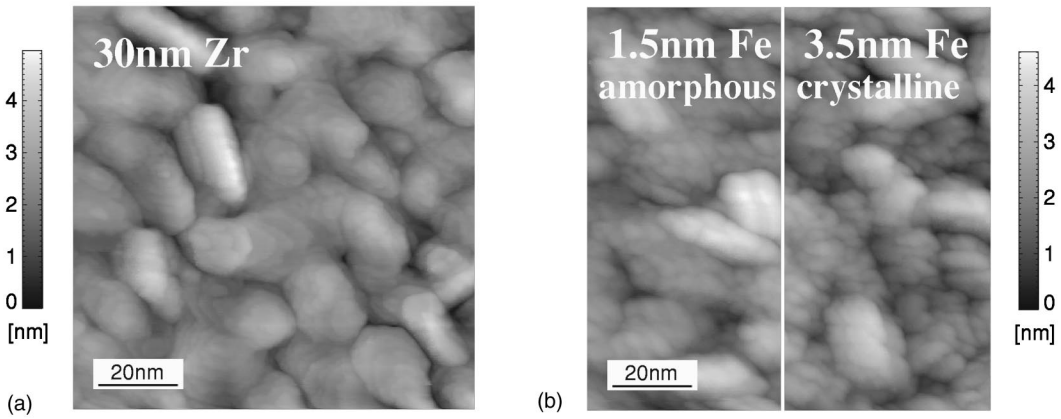

FIG. 1. Growth morphologies of thin Fe film on 30 nm Zr, in dependence of the film thickness.

takes place. The results are discussed in the framework of phase transition— and growth models, as well as previous results.

II. EXPERIMENTAL DETAILS

To exclude uncontrollable contamination effects, the films are prepared in UHV on Si(100) wafers with natural oxide using independently rate-controlled electron-beam evaporators (base pressure of the evaporation chamber $<3\times10^{-10}$ mbar) and are investigated *in situ*. First, 30-nm-thick Zr substrates are evaporated, and then on top of them the ZrFe films, using typical total evaporation rates of 0.2 nm/s. The typical error in the individual rates for the different materials is of the order of 0.01 nm/s, which corresponds to deviations in the stoichiometry of typically ±0.5 At%. During film deposition, the substrates are single-edge clamped, and a two-laser beam-deflection method is used for measuring the substrate curvature for determination of the film stresses. Using the biaxial stress model, which assumes vanishing stress components perpendicular to the substrate and isotropic strains in the plane of the film, force and momentum balance between the film and substrate result in the *Stoney* equation.[19] It relates the force per unit width $\tilde{F}$ (which are the integral stresses over the film thickness) to the substrate radius of curvature r (with the substrate biaxial elastic modulus B_S, the substrate thickness t_S and the film thickness t)

$$\tilde{F}(t)=\frac{B_S t_S^2}{6r}. \tag{2}$$

The stress $\sigma(t)$, at which a new layer of material grows at a particular film thickness, can thus be obtained by derivation

$$\sigma(t)=\frac{\partial\tilde{F}(t)}{\partial t}. \tag{3}$$

The application of the aforementioned relations requires the biaxial curvature of the substrate not to be hindered by the clamping mechanism[20] and the limit of small film thicknesses in comparison to the substrate, which is experimentally fullfiled for the present studies. Here, the convention of positive compressive stresses is applied.

Amorphicity is verified *in situ* with reflection high-energy-electron diffraction (RHEED). After transfer to a different chamber, without breaking the vacuum, STM measurements are preformed using electrochemically etched tungsten tips (typical tunneling conditions: $U_T\approx1$ V, $I_T\approx1$ nA). For a quantitative evaluation of the surface topographs, considered as a two-dimensional function $h(\vec{x})$ [$\vec{x}=(x,y)$] on a coordinate system parallel to the substrate with $\langle h(\vec{x})\rangle_{\vec{x}}=0$, the surface roughness

$$\zeta=\sqrt{\langle[h(\vec{x})]^2\rangle_{\vec{x}}} \tag{4}$$

as well as the height-height-correlation function (e.g., Ref. 21)

$$C(r)=\langle h(\vec{x})\cdot h(\vec{x}+\vec{R})\rangle_{\vec{x},|\vec{R}|=r} \tag{5}$$

are calculated. They allow to quantify both characteristic length scales in STM topographs, the structure height ζ, as well as the structure lateral size, which can be determined as abscissa R_C of the first maximum of $C(r)$.

III. POLYMORPHOUS GLASS TO CRYSTAL TRANSITION OF $Fe_{100-x}Zr_x$

The growth and crystallization behavior of initially amorphous, interface-stabilized $Fe_{100-x}Zr_x$ films, deposited on a 30-nm-thick Zr substrate is investigated in the region of the critical film thickness. Figure 1(a) shows the Zr substrate, on which in Fig. 1(b) a 1.5-nm pure Fe ($x=0$) is evaporated. As typical line scan [Fig. 2(a,b)] shows that this film is still amorphous. On reaching 3.5-nm film thickness [Fig. 1(b)], without doubt a crystal film can be observed. As can be seen in Fig. 2(c,d), the measurable step height (approximately 0.28 nm) agrees well with the lattice parameter of bulk bcc Fe (0.287 nm, Ref. 22). After crystallization, the size of the crystallites, as observable by STM, agrees very well with the size of single hills of the amorphous film, i.e., amorphous hills crystallize into individual single crystals. This growth and crystallization behavior, as described here for $x=0$, is observed also for all other investigated compositions, show-

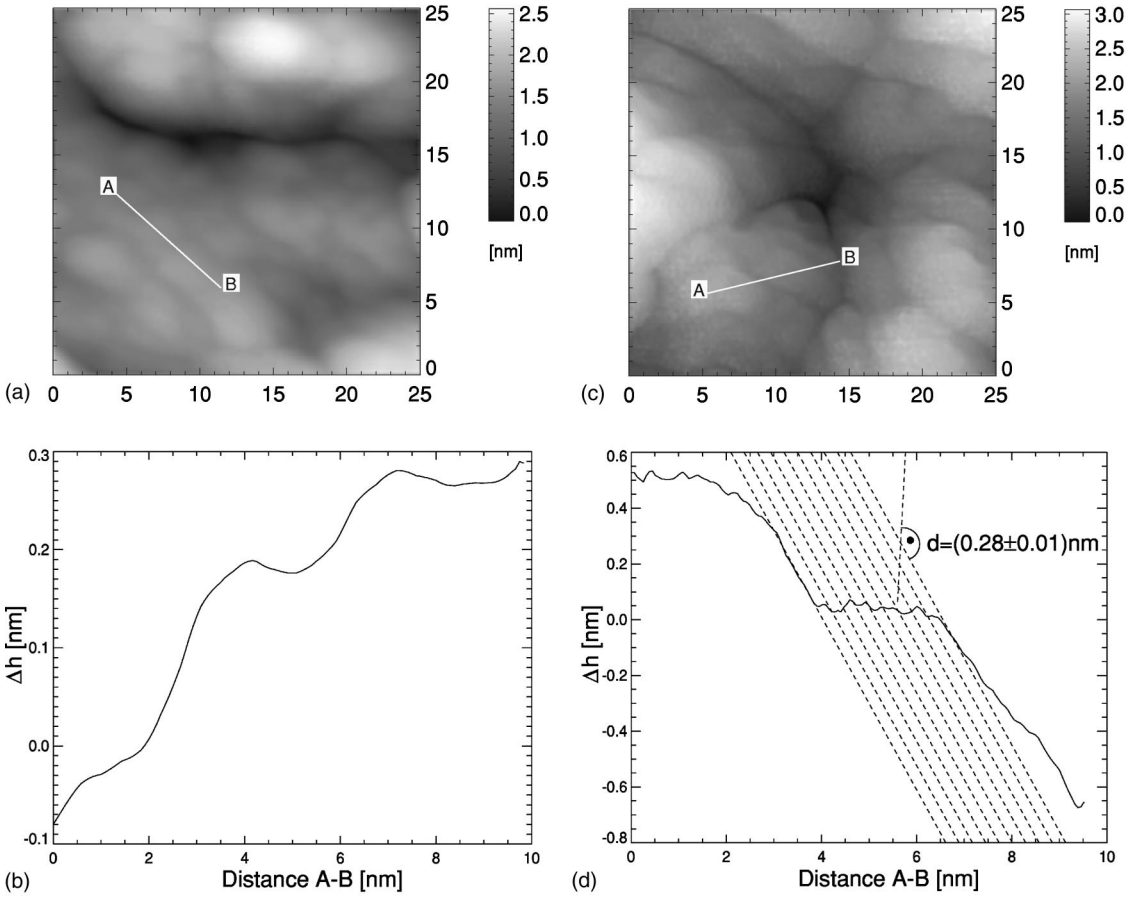

FIG. 2. Crystallization behavior of pure Fe film on Zr, exceeding the critical film thickness: (a,b): 1.5 nm Fe on 30 nm Zr; (c,d): 3.5 nm Fe on 30 nm Zr. The line scan (d) shows a tilted crystal; due to the different scaling of x and y axis, the expected 90° angle is distorted.

ing a glass to crystal transition at thicknesses in agreement with previous studies.[18]

Stress measurements by substrate-curvature measurements during the glass-to-crystal transition of $Fe_{100-x}Zr_x$ on 30 nm Zr prepared at room temperature, are hampered by the polycystallinity of the Zr film [Fig. 1(a)], as changes in the stress state of the $Fe_{100-x}Zr_x$ films on top of single Zr crystallites might not be fully transfered to the substrate. It is, therefore, desireable to prepare smoother Zr films, which can be achieved by raising the substrate temperature during the deposition of the 30-nm-thick Zr film due to the increased atomic mobility. In Fig. 3, a stress measurement is shown in dependence of the film thickness of a $Fe_{94}Zr_6$ film, prepared at room temperature on a 30-nm-thick Zr film, which has been previously evaporated at 773 K. A continous buildup of tensile stresses for film thicknesses higher than ≈ 30 nm can be observed, as discussed below in more detail, and a reproducible buckling of the stress curve, signalizing a volume decrease of the $Fe_{94}Zr_6$ film in the region of the polymorphous crystallization (film thickness ≈ 6 nm), as magnified in the inset (Fig. 3).

IV. FILM THICKNESS SERIES OF $Fe_{93}Zr_7$

Surface structure formation is investigated in dependence of the film thickness for $Fe_{93}Zr_7$ on a 30-nm-thick Zr substrate. Figure 4b (inset) shows characteristic STM topographs taken from a film thickness series. Starting from at least 120-nm film thickness, the film is crystalline, in accordance with RHEED and x-ray diffraction measurements. Concerning a quantitative evaluation, the roughness in dependence of the film thickness [Fig. 4(a)] shows a significant increase with increasing film thickness, with a reduced rate of the increase for film thicknesses higher than ≈ 100 nm. The lateral structure size R_C [Fig. 4(b)] of the Zr substrate is dominated by the Zr crystallites, on top of which $Fe_{93}Zr_7$ hills grow. The latter show an increase in their lateral size with the film thickness. The maximum of R_C at ≈ 50-nm film thickness directly corresponds to the point, when the $Fe_{93}Zr_7$ structures exactly cover the Zr crystallites of the substrate. Additional film growth generates a different lateral structure size on top of the Zr crystallites of the substrate, which finally saturates at ≈ 17 nm structure size. This kind of growth, where the lateral structure size saturates and the roughness increases for all film thicknesses, is characteristic for columnar polycrystalline growth.

For all investigated compositions, the growth described exemplary for $Fe_{93}Zr_7$ remains qualitatively valid. Generally, this kind of film growth is accompanied by the buildup of strong intrinsic tensile stresses, once three-dimensional growth occurs with constant lateral structure sizes, as already

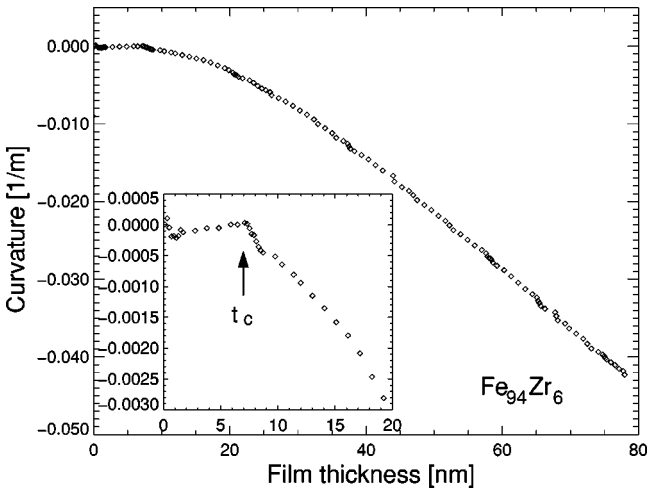

FIG. 3. Mechanical stresses during evaporation of $Fe_{94}Zr_6$ on top of 30 nm Zr, which has been deposited at 773 K on a Si(100) substrate. The *inset* shows a buckling of the stress curve in the region of polymorphous crystallization (at the critical film thickness t_C), which is reproducibly observable.

shown above. For the present composition, saturation stresses of at least 0.89 GPa can be determined.[23]

V. AMORPHOUS $Fe_{66.4}Zr_{33.6}$ FILM GROWTH

Switching to $x>7$ for $Fe_{100-x}Zr_x$ films under the applied deposition conditions, the polymorphous glass-to-crystal transition no longer takes place, and the films grow amorphous for any film thickness. This is particularly interesting, as thus a link of crystal growth to amorphous growth is possible, which—concerning film stresses and surface topography—is even quantitatively completely understood.[24,25] Figure 5 shows two STM topographs for 100-nm-thick films, prepared with deposition rates, which differ by one magnitude [Fig. 5(a) is evaporated using 0.04 nm/s and Fig. 5(b) using 0.4 nm/s]. Although the lateral structure size R_C, as determined from $C(r)$, of Fig. 5(a) ($R_C \approx 12.0$ nm) is a little smaller [$R_C \approx 12.2$ nm for Fig. 5(b)], there is no major difference from a statistical point of view in the surface topographs, proofing the primary independence of the present studies from the deposition rate within the experimentally accessible range.

Previous studies on various metallic glasses revealed that the three-dimensional kind of growth with mesoscopic hill-like structures (as in Fig. 5) is accompanied by strong tensile stresses.[25] From a qualitative point of view of the surface topographs and film stresses, amorphous and crystal systems, therefore, do not differ too much, if the amorphous mesoscopic hills are identified with single crystallites of the polycrystal film in the sense that in both cases growth instabilities occur, leading to roughening and three-dimensional growth. The latter then is the basis for continuous-structure coalescence, which can be deemed to be the reason for tensile stress formation.[26,25]

VI. INTERDIFFUSION OF Zr/$Fe_{94}Zr_6$ DOUBLE LAYERS

Film stresses and the composition of the top film layers (using Auger electron spectroscopy—AES) are measured

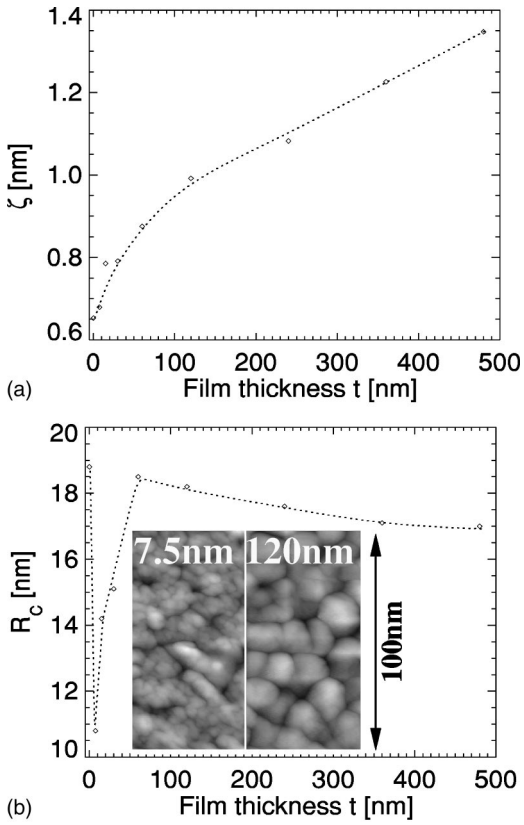

FIG. 4. Film thickness series of $Fe_{93}Zr_7$, which is cocondensed with 0.23 nm/s on Zr: Roughness ζ (a), correlation lengths R_C (b), and typical surface topographs (*inset*).

during deposition of $Fe_{94}Zr_6$ at different substrate temperatures on a 30-nm-thick Zr film, which had been previously prepared at room temperature. As the morphology of the Zr layers does not change significantly during annealing at the experimentally accessible temperatures, this ensures comparable conditions for the deposition of $Fe_{94}Zr_6$ at different substrate temperatures. Figure 6 shows the temperature dependence of the evolution of the film stresses during deposition of $Fe_{94}Zr_6$ on Zr, where bimetal stresses of the Zr films on the Si(100) substrates are eliminated. The late stages of growth are characterized by a pronounced buildup of tensile saturation stresses, which decrease in their magnitude with increasing substrate temperature, as it is characteristic for the temperature behavior of tensile stresses occuring during columnar film growth.[27,28] The latter has been shown above to be present here. Early-stage compressive stresses occur with increasing temperature, starting at ≈ 323 K. They can be understood, considering Fig. 7, showing Auger spectra of the top films of nominal composition $Fe_{94}Zr_6$: With increasing temperature the spectra are enriched with Zr, which is a strong indication of Fe diffusion into the subjacent Zr film, generating compressive stresses. This is particularly obvious due to the small-grained microstructure of the Zr layer, as grain boundaries, tripple points, or even dislocations and point defects can promote interdiffusion by magnitudes[29–31] in comparison to bulk diffusion. Vice versa, the missing compressive stress generation at room temperature is thus a

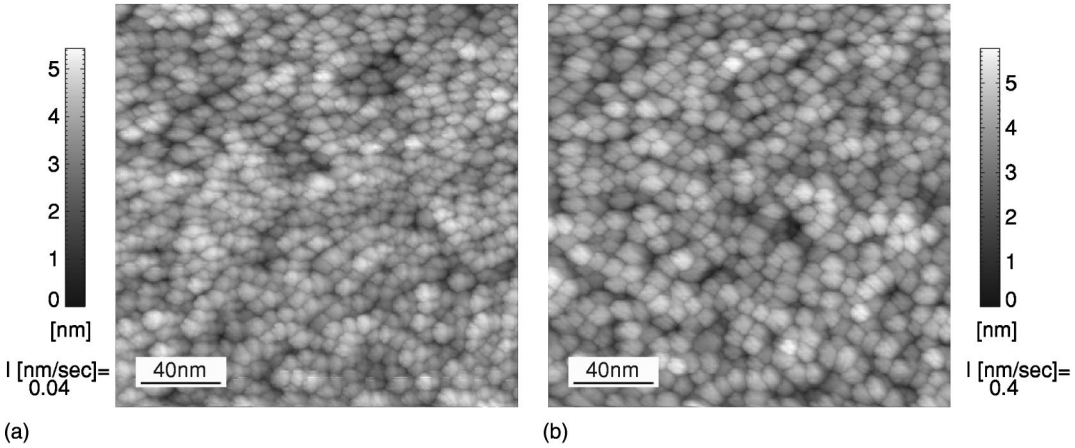

FIG. 5. Evaporation of 100-nm-thick amorphous $Fe_{66.4}Zr_{33.6}$ films, with deposition rates I, differing by one magnitude.

strong indication for the absence of interdiffusion (and thus a solid-state amorphization reaction) at room temperature.

VII. DISCUSSION

A. Polymorphous crystallization

The temperature-dependent stress measurements presented here (Fig. 6) directly prove that amorphization in the thin film thickness regime for ZrFe on Zr does not originate from a solid-state amorphization reaction, but has its origin in a destabilization of the crystalline state due to interface effects, as has been considered in literature before (e.g., Refs. 8,13,5,6). This is corroborated by STM topographs (Fig. 1), which show just ZrFe on top of the Zr substrate without any change of the morphology by diffusion. In the following, we discuss the nature of the underlying phase transition in the framework of instabilities, which is of general interest for any kind of polymorphous amorphization or melting. For convenience, we thermodynamically treat the polymorphous crystallization of the ZrFe films on Zr under constant pressure, i.e., as a quasi-free-standing film, however, including the ZrFe/vacuum and ZrFe/Zr interface energies. This can be justified, as the elastic energy-density contribution during phase transformation $\Delta g = V_m(\Delta\sigma)^2/B \approx 0.7$ J/mol, with the biaxial modulus of Fe $B = 295$ GPa (Ref. 32), the molar volume V_m and $\Delta\sigma \approx 0.17$ GPa, is completely negligible in comparison to the other bulk and interfacial driving forces in the magnitude of kJ/mol.[17] Using the relation[33]

$$\Delta\sigma = \frac{B}{3}\frac{\Delta V}{V_0}, \tag{6}$$

a relative change of volume of 0.17% can be estimated, assuming that possible interface stress contributions can be neglected. This means that at the critical thickness of polymorphous crystallization the volume change is very small in comparison to bulk samples, which can exhibit volume changes up to 2%.[34] Following Tallon,[35] we describe the entropy of the glassy state as a liquid without communal entropy, which can be estimated using the isothermal volume dependence

$$\left(\frac{\partial S}{\partial V}\right)_T = \frac{\alpha}{\kappa_T}, \tag{7}$$

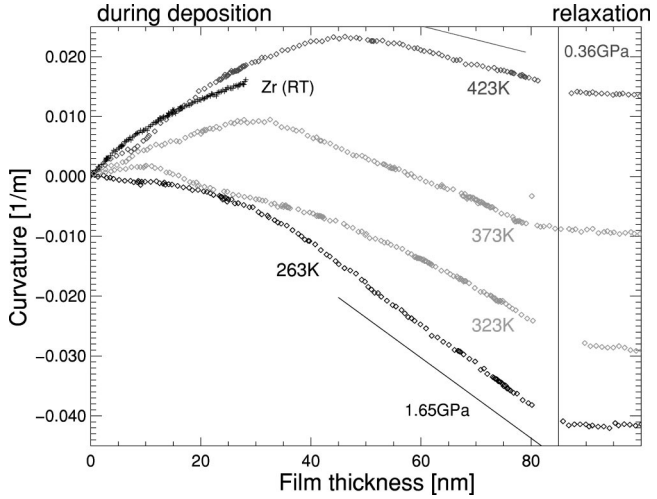

FIG. 6. Mechanical stresses during condensation of 80 nm $Fe_{94}Zr_6$ on 30 nm Zr in dependence of the substrate temperature.

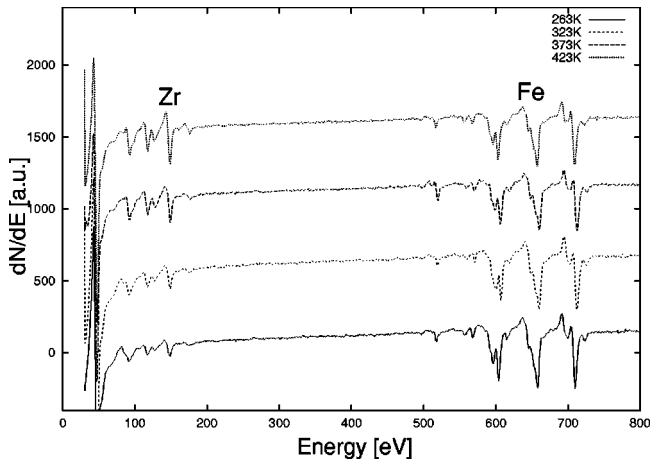

FIG. 7. AES in dependence of the substrate temperature for $Zr/Fe_{94}Zr_6$ double layers.

where α and κ_T are the isothermal volume expansion and compressibility, respectively, assummed to be of the same magnitude in the crystal and liquid phase. Within this approximation, we therefore find a vanishing enthropy difference between the crystal and glass, due to the vanishing volume change $\Delta V \approx 0$

$$\Delta S = \frac{\alpha}{\kappa_T} \Delta V \approx 0. \tag{8}$$

This suggests that the glass-to-crystal transition happens near a catastrophic point similar to suggestions of Kautzmann[36] that the glass transition occurs at a point where the enthropy of a supercooled liquid equals that of a crystal. For the present studies, this point coincides with a catastropic point suggested by Tallon[35] for melting of close-packed structures, where the crystal and amorphous density agree, although the present crystal structure is bcc. Indeed, a vanishing volume change can be seen in direct relation to Born's description of the crystal-to-glass transition as a shear instability,[37] where the volume can be expected to be primarily conserved. In this context, it should be pointed out that our observations of almost no abrupt density change and thus a vanishing latent heat are in complete contrast to ordinary crystallization phenomena.

The growth morphology of the amorphous films has significant influence on the transformation: The presence of mesoscopic hilllike structures, with corrugations in the magnitude of the film thickness, will lead to preferential nucleation in the center of a mesoscopic hill, as the critical thickness is first reached there. With additional deposition of material, the grains can be expected to extend laterally, forming grain boundaries at the grooves between the initially amorphous hills, until the critical film thickness is reached throughout the film. Thus, also the grain boundary energy can be reduced. Based on this picture, the ≈ 2-nm-thickness regime of phase transformation in Fig. 3 is a measure for the surface corrugations, which indeed agrees very well with the STM topographs (Fig. 1). Additional experimental evidence is that amorphous mesoscopic structure size matches the crystallite size after the phase transition (Fig. 2). Thus, different critical thicknesses can be measured for different preparation conditions, as can be also concluded from the varying results in literature for pure Fe on Zr (e.g., Refs. 8,13,5,6).

B. Film growth morphologies and kinetics

Considering all of the aforementioned experimental facts, it is possible to identify the main features of $Fe_{100-x}Zr_x$ growth on Zr: Independent of the details of the composition, the first layers on Zr grow islandlike. As Fe reveals a lower melting point than Zr, and as the system ZrFe has a high negative heat of mixing,[38] wetting behavior should be expected contrary to this experimental fact. This allows one to identify the growth kinetics as the dominant structure-forming aspect for ultrathin films on Zr, i.e., a self-shadowing behavior, where—starting from one initially deposited atom—additional atoms are deflected towards it, thus building up a mesoscopic hill, as suggested in Refs. 39 and 24. Further growth is primarily influenced by the composition and substrate temperature: If the $Fe_{100-x}Zr_x$ composition is less than $x \leqslant 7$, polymorphous crystallization takes place at a critical thickness, where single hills crystallize to single nanocrystallites. For higher concentration of x (either due to the deposition stoichiometry or due to Fe diffusion into Zr), the islands remain amorphous. Concerning the further film growth, on a mesoscopic scale no major difference between polycrystal or amorphous film growth exists from a qualitative point of view. In both cases the self-shadow instability leads to a three-dimensional growth, which is responsible for tensile film stresses due to continuous structure coalescence. The possibility of stabilizing monoatomic amorphous Fe films on Zr, allows the interesting chance of STM studies on monoatomic amorphous structures on an atomic scale. As Fig. 2(a) with observable structures of several nanometers in lateral size suggests, under the applied tunneling conditions, single atoms are not observed. As previously suggested,[40] the structures on top of the mesoscopic hills can be identified as localized electron waves, observable either due to local short-range ordering or exposed surface atoms. However, the clear distinctness between amorphous and crystal surfaces on scales of the mesoscopic islands of a few nanometers, suggests that even on this scale amophous and crystal solids are profoundly different.

VIII. CONCLUSIONS

The experiments presented in the present work provide direct evidence of interface-stabilized amorphous film growth of ZrFe-alloy films on Zr substrates under different bulk driving force at room temperature. Below a critical threshold thickness, the interface effects clearly dominate. Additional increase of the film thickness above the critical value leads to crystallization under almost neglectable volume change, which can be understood in terms of catastrophic instabilities. For increased substrate temperature, interdiffusion takes place, and the observable amorphization along the interface can be expected to be significantly influenced by solid-state amorphization. With further increase in the film thickness, both, in pure crystal, as well as solely amorphous films, a clusterlike surface morphology evolves, where for crystals the clusters can be identified with single crystallites. This kind of three-dimensional growth in both cases is accompanied by intrinsic tensile stress generation due to continuous cluster coalescence. In summary, by interface effects, shifting the equilibium phase diagrams, it is possible to tailor phases, normally not accessible for applications, and to study phase transformations in thin films.

ACKNOWLEDGMENTS

The authors acknowledge U. Herr for fruitful discussions, as well as A. Grob for previous results.

*Present address: Department of Materials and Engineering, University of Illinois at Urbana-Champaign, 405 W. Green Street, Urbana, Illinois 61801. Email address: smayr@uiuc.edu

[1] R.B. Schwarz and W.L. Johnson, Phys. Rev. Lett. **51**, 415 (1983).
[2] B.M. Clemens and M.J. Suchoski, Appl. Phys. Lett. **47**, 943 (1985).
[3] H. Geisler, U. Herr, and K. Samwer, Thin Solid Films **275**, 176 (1996).
[4] T. Otto, T. Stobiecki, F. Stobiecki, and K. Röll, J. Magn. Magn. Mater. **101**, 207 (1991).
[5] Y. Kudryavtsev, J. Dubrowik, and F. Stobiecki, Thin Solid Films **256**, 171 (1994).
[6] J. Dubowik, J. Magn. Magn. Mater. **140-144**, 531 (1995).
[7] U. Herr, H. Ippach, and K. Samwer, Appl. Phys. Lett. **75**, 1730 (1999).
[8] D.E. Williamson and B.M. Clemens, Hyperfine Interact. **42**, 967 (1988).
[9] W. Kiauka, W. Keune, T. Shinjo, and N. Hosoito, J. Magn. Magn. Mater. **93**, 494 (1991).
[10] A. Paesano, S.R. Teixeira, and L. Amaral, J. Appl. Phys. **70**, 4870 (1991).
[11] W. Buckel and R. Hilsch, Z. Phys. **138**, 109 (1954).
[12] C.L. Chien, S.H. Liou, and G. Xiao, in *Metallic Multilayers and Epitaxy*, edited by M. Hong, D.G. Gubser, and S.A. Wolf (TMS, Warrendale, 1989), p. 245.
[13] W. Kiauka, C. van Cuyck, and W. Keune, Mater. Sci. Eng., B **B12**, 273 (1992).
[14] B.M. Clemens, J. Less-Common Met. **140**, 57 (1988).
[15] J. Landes, C. Sauer, B. Kabius, and W. Zinn, Phys. Rev. B **44**, 8342 (1991).
[16] J. Thile *et al.*, J. Magn. Magn. Mater. **119**, 141 (1993).
[17] U. Herr, H. Geisler, H. Ippach, and K. Samwer, Phys. Rev. B **59**, 13 719 (1999).
[18] U. Herr, Contemp. Phys. **41**, 93 (2000).
[19] G.G. Stoney, Proc. R. Soc. London, Ser. A **82**, 172 (1909).
[20] K. Dahmen, S. Lehwald, and H. Ibach, Surf. Sci. **446**, 161 (2000).
[21] G. Rasigni *et al.*, Phys. Rev. B **27**, 819 (1983).
[22] C. Kittel, *Einführung in die Festkörperphysik* (R. Oldenbourg Verlag, München, Wien, 1991).
[23] A. Grob, U. Herr, and K. Samwer, J. Metastable and Nanocrystalline Materials **8**, 243 (2000).
[24] S.G. Mayr, M. Moske, and K. Samwer, Phys. Rev. B **60**, 16 950 (1999).
[25] S.G. Mayr and K. Samwer, Phys. Rev. Lett. **87**, 036105 (2001).
[26] W.D. Nix and B.M. Clemens, J. Mater. Res. **14**, 3467 (1999).
[27] R.W. Hoffman, *Physics of Thin Films—Advances in Research and Development* (Academic Press, New York, 1966), p. 211.
[28] J.A. Thornton and D.W. Hoffman, Thin Solid Films **171**, 5 (1989).
[29] K. Samwer, Phys. Rep. **161**, 1 (1988).
[30] K. Samwer, H. J. Fecht, and W.L. Johnson, in *Glassy Metals III*, edited by H. Beck and H.-J. Güntherodt (Springer-Verlag, Berlin, 1994).
[31] S. Schneider, R. Busch, W. Bolse, and K. Samwer, J. Non-Cryst. Solids **156**, 498 (1993).
[32] G. Simmons and H. Wang, *Single Crystal Elastic Constants and Calculated Aggregate Properties* (MIT Press, Cambridge, MA, 1971).
[33] O.B. Loopstra, E.R. van Snek, T.H. de Keijser, and E.J. Mittemeijer, Phys. Rev. B **44**, 13 519 (1991).
[34] U. Köster and U. Herold, in *Glassy Metals I*, edited by H. Beck and H.-J. Güntherodt (Springer-Verlag, Berlin, 1981).
[35] J. Tallon, Nature (London) **342**, 658 (1989).
[36] W. Kautzmann, Chem. Rev. **43**, 219 (1948).
[37] M. Born, J. Chem. Phys. **7**, 591 (1939).
[38] F. Gärtner, C. Michaelsen, and R. Bormann, Philos. Mag. B **76**, 511 (1997).
[39] N.J. Shevchik, J. Non-Cryst. Solids **12**, 141 (1973).
[40] T.M. Schaub, D.E. Bürgler, C.M. Schmidt, and H.-J. Güntherodt, J. Non-Cryst. Solids **205–207**, 748 (1996).